CHIN. PHYS. LETT. Vol. 36, No. 7 (2019) 077402 **Express Letter**

Observation of Two-Level Critical State in the Superconducting FeTe Thin Films*

Hao Ru(茹浩), Yi-Shi Lin(林一石), Yin-Cong Chen(陈寅聪), Yang Feng(冯洋), Yi-Hua Wang(王熠华)**

Department of Physics and State Key Laboratory of Surface Physics, Fudan University, Shanghai200438

(Received 12 June 2019)

FeTe, a non-superconducting parent compound in the iron-chalcogenide family, becomes superconducting after annealing in oxygen. Under the presence of magnetism, spin-orbit coupling, inhomogeneity and lattice distortion, the nature of its superconductivity is not well understood. Here we combine the mutual inductance technique with magneto transport to study the magnetization and superconductivity of FeTe thin films. It is found that the films with the highest T_C show non-saturating superfluid density and a strong magnetic hysteresis distinct from that in a homogeneous superconductor. Such a hysteresis can be well explained by a two-level critical state model and suggests the importance of granularity to superconductivity in this compound.

PACS: 74.25.Ha, 74.25.F−, 74.78.−w, 74.70.Xa DOI: 10.1088/0256-307X/36/7/077402

Iron-chalcogenide is an important family of iron-based high T_C superconductors (Fe-SCs). It has the simplest crystal structure with one layer of Fe square lattice sandwiched between two layers of chalcogen atoms. Despite the simplicity of its crystal structure, a single layer of FeSe grown on $SrTiO_3$ displays the highest T_C among Fe-SCs.[1] While the electronic structures are similar across Fe-SCs, the magnetic structure in the Fe square lattice is complex and intriguing,[2,3] and is believed to be essential for the pairing interaction in Fe-SCs.[4] As spin-fluctuations on the FeSe side evolve into an antiferromagnetic ordering on the FeTe side, superconductivity disappears. Furthermore, in the presence of stronger spin-orbit coupling at higher Te concentration, the band structure of iron-chalcogenides has shown non-trivial topology[5] and the vortex cores of the superconducting compounds have shown signs of zero-bias peaks.[6] Inducing superconductivity in FeTe is therefore useful for both the understanding of its relation with magnetism and utilizing even stronger spin-orbit coupling in iron-chalcogenide family.

It has been reported that FeTe films may become superconducting after annealing in oxygen[7] or simply being exposed to air for a long time.[8] The oxygen atoms occupy the interstitial sites in the Te planes and substituting Te with O would only suppress superconductivity.[9] Exposing a bulk crystal to oxygen could not show the similar effect,[10] suggesting that the substrate plays a role in inducing superconductivity. Nevertheless, superconductivity has been found in FeTe films grown on different substrates,[7,8,10] even those that do not necessarily match the crystal symmetry and lattice constant of FeTe.[7,10] The exact roles of oxygen and substrate in inducing the superconductivity in FeTe and whether such superconductivity bears any resemblance to other compounds in the iron-chalcogenide family remain largely unknown.

In this Letter, we report the observation of two-level critical state in the superconducting FeTe thin films grown on Al_2O_3. We combine the mutual inductance technique with magneto transport to uncover the surface resistance change over 8 decades when the superconductivity is tuned by temperature and magnetic field. Despite a T_C of around 13 K, superfluid density does not saturate down to 2 K. Furthermore, the films show magnetic hysteresis in surface resistance distinctively different from what one might expect from a homogeneous superconductor with vortex pinning. The hysteresis decreases with increasing temperature and with reducing maximum magnetic field in a way consistent with the two-level critical state model. These observations suggest the importance of granularity for the superconductivity in FeTe thin films induced by oxygen.

In experiment, we grew FeTe thin films using molecular-beam-epitaxy on both Al_2O_3 and $SrTiO_3$ substrates and annealed the sample *in situ* in an oxygen pressure of about 10^{-2} Torr (see the supplementary materials). The films on the latter substrate show better morphology (see the supplementary materials) but much lower or even zero T_C. The current study focuses on the films grown on Al_2O_3 and use a film of 49 nm thick as a representative throughout this paper. Its resistance shows a superconducting transition around 13 K (Fig. 1(a)) and shows a down turn at around 70 K (Fig. 1(a) inset). The latter one is also present in the non-superconducting FeTe bulk crystals and is associated with the antiferromagnetic transition.[11]

In order to investigate the superconducting regime below 10 K where the resistance of the film would be too small to be reliably measured using charge transport (Fig. 1(a)), we employed the mutual inductance technique, which is sensitive to the superconductiv-

*Supported by the National Key Research and Development Program of China under Grant Nos 2016YFA0301002 and 2017YFA0303000, and the National Natural Science Foundation of China under Grant No 11827805.

**Corresponding author. Email: wangyhv@fudan.edu.cn

© 2019 Chinese Physical Society and IOP Publishing Ltd

ity even in monolayer films.[12,13] The in-phase component of the ac voltage on the pickup coil V_p increases whereas the out-of-phase component decreases with temperature below 10 K (Fig. 1(b)), in consistent with a diamagnetic response.[14–17] However, unlike the diamagnetic response of a BCS bulk superconductor, the in-phase component exhibits a broad peak and the out-of-phase component does not saturate down to 2 K (Fig. 1(b)). Such behavior has been observed in other unconventional superconducting films.[14,17]

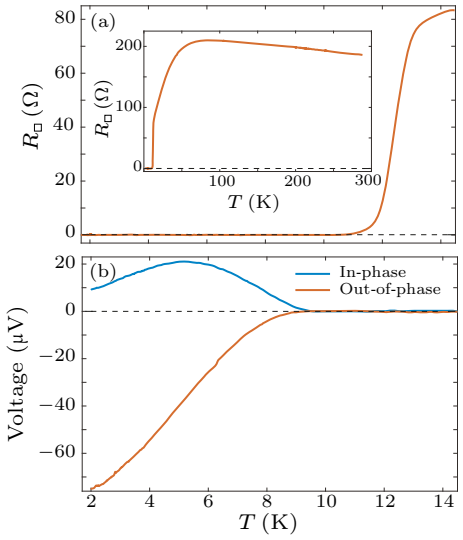

Fig. 1. Unsaturated superconductivity in FeTe films after annealing in oxygen. (a) The sheet resistance $R_\square$ of a 49-nm-thick FeTe sample after annealed in oxygen. Inset: resistance over a larger temperature range showing a transition around 70 K similar to the antiferromagnetic transition in the non-superconducting FeTe bulk crystals. (b) The mutual inductance signal of the same sample. Blue and orange are the in-phase and out-of-phase components of the ac voltage signal on the pickup coil (see the supplementary materials), respectively. The data were obtained at a drive frequency of 10 kHz and drive current of 10 μA.

As a function of the external magnetic field applied perpendicular to the film, our sample shows strong hysteresis both from transport and from mutual inductance measurement (Fig. 2). The overall signal is symmetric about zero field, and therefore we focus our discussion on the positive field. At 2 K, resistance in the down-sweep (Fig. 2(a) blue) is lower than that in the up-sweep (Fig. 2(a) orange), leading to an enhanced critical field in the down-sweep. Similarly, the out-of-phase component of the mutual inductance signal is also lower in the down-sweep than in the up-sweep (Fig. 2(b)), leading to a peak value in the down-sweep occurring at ~0.2 T before the field returning to zero. The magnitude of the hysteresis as represented by the difference between up and down sweeps decreases as temperature increases (Fig. 2(d)). Due to the reduced in-phase and out-of-phase signals close to T_C, no hysteresis is observable from the mutual inductance signal above 9 K (Figs. 2(b)–2(d)). Nevertheless, it is still present in the resistance data up to 11 K (Fig. 2(a) inset).

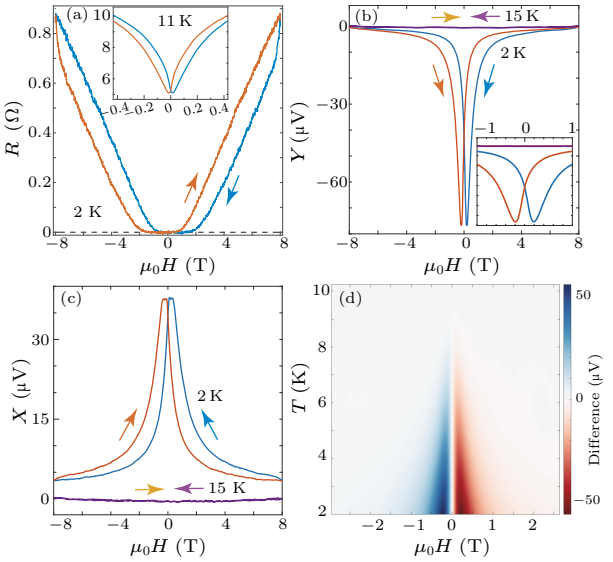

Fig. 2. Magnetic hysteresis of the film in the superconducting state. (a) Resistance at 2 K (inset: 11 K) showing hysteresis under up-sweep (orange) and down-sweep (blue) of the perpendicular magnetic field. The sample was cooled under nominally zero field to 2 K. Similar hysteresis is observed from the mutual inductance measurement on the out-of-phase (b) and in-phase (c) components. The yellow and purple curves, which overlap, represent up and down sweeps, respectively, at 15 K. (d) Difference between the down and up field sweeps of out-of-phase component of the mutual inductance signal as a function of temperature.

We find that the magnetic hysteresis in the superconducting state obtained from both transport and mutual inductance signal could be unified if we transform the mutual inductance voltage $V_p = X + iY$ into surface impedance $Z_s = R_s + i\omega L$ according to

$$V_p = i\omega I_d \int_0^\infty dx \frac{M(x)}{1 - (\frac{2xi}{\mu\mu_0 h\omega})Z_s},$$

where R_s is the surface resistance, L is the inductance with $L^{-1} = (\frac{2e^2}{m})n_s$ proportional to superfluid density n_s, I_d and ω is the amplitude and frequency of the drive current, respectively, and $M(x)$ is determined by the specific geometry of the mutual inductance coils.[16,17] We used frequencies around 10 kHz for both transport and mutual inductance measurements to keep them in a similar quasi-dc regime. As we can see from Fig. 3(a), $R_s(T)$ can be connected with $R(T)$ from transport up to a scaling constant. They overlap in the temperature window of 10–11 K, below which the resistance in the superconducting state is too small to be measured by charge transport and above which the surface impedance is dominated by normal inductance. Combining $R_s(T)$ and $R(T)$, we can cover 8 decades of variation in resistance from the first sign of superconductivity at 13 K. From the imaginary part of Z_s, we obtain L^{-1}, which shows that the superfluid density is almost kept in a linear

temperature dependence deep into the superconducting state and is unsaturated at 2 K (Fig. 3(b)). Such a linear dependence of $n_s(T)$ has been observed in cuprate superconductors.[14,18]

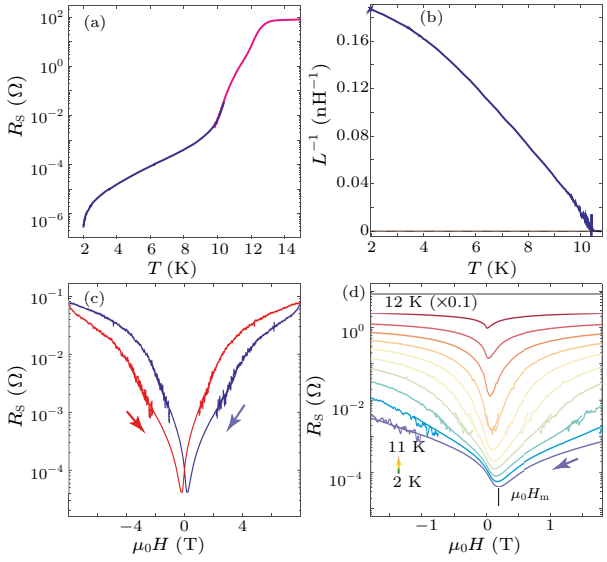

Fig. 3. Obtaining surface impedance and the magnetic hysteresis in the surface resistance. (a) Surface resistance R_s of the superconducting film as a function of temperature, measured by transport (magenta) and extracted from mutual inductance (purple). (b) Inverse of the surface inductance (which is proportional to the superfluid density) extracted from the mutual inductance data. See text for the details for extracting the surface impedance from mutual inductance data. (c) R_s as a function of magnetic field. Again, the data in the high field region are obtained from transport and the data in the low field region are extracted from surface impedance. The maximum applied field ($\mu_0 H_{max}$) is 8 T. (d) Field down-sweep of R_s as a function of temperature with $\mu_0 H_{max} = 8$ T. The 12 K data (grey) are scaled down by a factor of 10. Here $\mu_0 H_m$ is defined as the field at which the lowest R_s occurs in the down sweep.

Applying the same method on the mutual inductance data under sweeping external magnetic field H at various fixed temperatures (Figs. 2(b), 2(c) and 2(d)), we are able to connect $R_s(H)$ from the mutual inductance with $R(H)$ from transport (Fig. 3(c) and 3(d)) using the same scaling constant for connecting the temperature data (Fig. 3(a)). The combined $R_s(H)$ hysteresis loop (Fig. 3(c)) clearly illustrates two abnormal features: (1) The surface resistance is lower in the down sweep, and (2) the minimum of the surface resistance occurs at a field H_m before the field crosses zero. These features are quite opposite to those expected from the hysteresis loop of a homogeneous superconductor with vortex pinning. Because R_s is caused by motion of the free vortices, such features in hysteresis suggest the existence of different levels of pinning strength which may be a result of granularity.[19]

According to the two-level critical state model, the intergranular regions have a higher penetration field H_g and much stronger pinning than the grain boundaries. When the field is swept upward, flux penetrates into grain-boundaries to first form Josephson vortices, which causes large increase in R_s due to a lower viscosity. In the down sweep, intergranular fluxons disappear first, leaving the more strongly pinned intragrain fluxons that contribute less R_s per fluxon than their intergranular counterparts.

The validity of the two-level critical state model can be further seen from the variation of hysteresis with the variation of temperature and maximum applied field H_{max}. As we increase temperature, both the magnitude of hysteresis in R_s and H_m reduce and both disappear at 12 K (Fig. 3(d)). H_m follows a linear temperature dependence (Fig. 4(a)), which suggests that the penetration field in the grains and the critical current density decrease linearly with increasing temperature. At the lowest temperature, H_m follows a linear dependence of H_{max} when it is small and tends to a constant when H_{max} is large (Fig. 4(b)). The turning point of these two regions is nothing but the grain's penetration field H_g, which can be determined by fitting H_m in the low field and by finding its interception point with the constant level at high field.[19] All these behaviors are in good agreement with the two-level critical state model.[19]

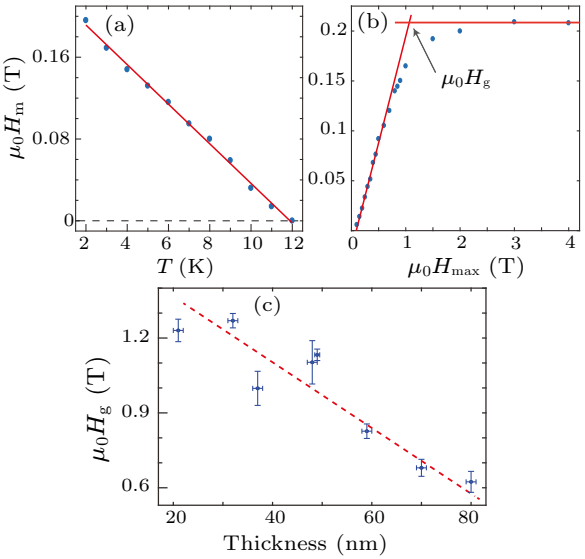

Fig. 4. Determination of the characteristic field in the two level critical state and its film thickness dependence. (a) The lowest field at which the lowest resistance occurs in the magnetic hysteresis H_m as a function of temperature obtained from Fig. 3(d). The red line is a linear fit. (b) H_m as a function of H_{max} measured at 2 K. The two red lines are linear fits in the high and low field regions, respectively. We can obtain the penetration field H_g from the crossing point between these two lines (see text). (c) H_g at 2 K as a function of film thickness. Films under comparison have similar T_C. The dashed line is a linear fit to guide the eyes.

We find that such a two-level critical state invariably occurs in the superconducting FeTe films we studied. Films of same thickness with higher T_C tend to have stronger hysteresis at same temperature, which

unsurprisingly gives the temperature dependence of $H_{\rm m}$ (Fig. 4(a)). What is a bit surprising is that $H_{\rm g}$ decreases in thicker films that have very similar $T_{\rm C}$ with the others under comparison (Fig. 4(c)). In the two-level critical state model, $H_{\rm g}$ is proportional to the grain size.[19] Our observation suggests that superconducting grains are much bigger in thinner FeTe films, which is in contrast to the roughness from topography (see the supplementary materials). This points suggestively to the role of both oxygen and interface in inducing superconductivity in FeTe: thinner films allow oxygen to permeate uniformly towards the bottom layers, whose lattice is likely distorted from the FeTe bulk, and this combination facilitates larger superconducting grains to form.

It is well known that granularity strongly affects the electromagnetic properties of superconductors. Even in high quality cuprate high $T_{\rm C}$ superconductors, granularity plays a crucial part in determining the critical density,[20,21] magnetization,[19] superfluid density[18] and superconducting gap inhomogeneity.[22] In some cases, granularity in thin films may appreciably enhance $T_{\rm C}$.[23,24] Our finding of the two-level critical state in the superconducting FeTe films after oxygen annealing suggests that granularity may also play an essential role in inducing superconductivity from an antiferromagnetically ordered iron-chalcogenide.

References

[1] Wang Q Y, Li Z, Zhang W H, Zhang Z C, Zhang J S, Li W, Ding H, Ou Y B, Deng P, Chang K, Wen J, Song C L, He K, Jia J F, Ji S H, Wang Y Y, Wang L L, Chen X, Ma X C and Xue Q K 2012 *Chin. Phys. Lett.* **29** 037402

[2] Carlson E W, Kivelson S A, Orgad D and Emery V J 2004 *Concepts in High Temperature Superconductivity* (Berlin: Springer) p 275

[3] Dai P 2015 *Rev. Mod. Phys.* **87** 855

[4] Davis J C S and Lee D H 2013 *Proc. Natl. Acad. Sci. USA* **110** 17623

[5] Zhang P, Yaji K, Hashimoto T, Ota Y, Kondo T, Okazaki K, Wang Z, Wen J, Gu G D, Ding H and Shin S 2018 *Science* **360** 182

[6] Yin J X, Wu Z, Wang J H, Ye Z Y, Gong J, Hou X Y, Shan L, Li A, Liang X J, Wu X X, Li J, Ting C S, Wang Z Q, Hu J P, Hor P H, Ding H and Pan S H 2015 *Nat. Phys.* **11** 543

[7] Nie Y, Telesca D, Budnick J I, Sinkovic B and Wells B O 2010 *Phys. Rev. B* **82** 020508(R)

[8] Si W, Jie Q, Wu L, Zhou J, Gu G, Johnson P D and Li Q 2010 *Phys. Rev. B* **81** 092506

[9] Hu H, Kwon J H, Zheng M, Zhang C, Greene L H, Eckstein J N and Zuo J M 2014 *Phys. Rev. B* **90** 180504(R)

[10] Han Y, Li W Y, Cao L X, Wang X Y, Xu B, Zhao B R, Guo Y Q and Yang J L 2010 *Phys. Rev. Lett.* **104** 017003

[11] Liu T J, Hu J, Qian B, Fobes D, Mao Z Q, Bao W, Reehuis M, Kimber S A J, Prokeš K, Matas S, Argyriou D N, Hiess A, Rotaru A, Pham H, Spinu L, Qiu Y, Thampy V, Savici A T, Rodriguez J A and Broholm C 2010 *Nat. Mater.* **9** 718

[12] Logvenov G, Gozar A and Bozovic I 2009 *Science* **326** 699

[13] Zhang Z, Wang Y H, Song Q, Liu C, Peng R, Moler K A, Feng D L and Wang Y Y 2015 *Sci. Bull.* **60** 1301

[14] Bozovic I, He X, Wu J and Bollinger A T 2016 *Nature* **536** 309

[15] Fiory A T, Hebard A F, Eick R H, Mankiewich P M, Howard R E and O'Malley M L 1990 *Phys. Rev. Lett.* **65** 3441

[16] Clem J R and Coffey M W 1992 *Phys. Rev. B* **46** 14662

[17] Fiory A T, Hebard A F, Mankiewich P M and Howard R E 1988 *Appl. Phys. Lett.* **52** 2165

[18] Deepwell D, Peets D C, Truncik C J S, Murphy N C, Kennett M P, Huttema W A, Liang R, Bonn D A, Hardy W N and Broun D M 2013 *Phys. Rev. B* **88** 214509

[19] Ji L, Rzchowski M S, An, N and Tinkham M 1993 *Phys. Rev. B* **47** 470

[20] Clem J R and Hao Z 1993 *Phys. Rev. B* **48** 13774

[21] Nguyen P P, Oates D E, Dresselhaus G and Dresselhaus M S 1993 *Phys. Rev. B* **48** 6400

[22] Kang M, Blumberg G, Klein M V and Kolesnikov N N 1996 *Phys. Rev. Lett.* **77** 4434

[23] Cohen R W and Abeles B 1968 *Phys. Rev.* **168** 444

[24] Shalnikov A 1938 *Nature* **142** 74

Supplementary Materials: Observation of Two-Level Critical State in the Superconducting FeTe Thin Films

Hao Ru(茹浩), Yi-Shi Lin（林一石）, Yin-Cong Chen(陈寅聪), Yang Feng(冯洋), Yi-Hua Wang(王熠华)*

Department of Physics and State Key Laboratory of Surface Physics, Fudan University, Shanghai 200438

* Correspondence author. Email: wangyhv@fudan.edu.cn

A: Materials and Methods

1. MBE growth of FeTe films on sapphire and $SrTiO_3$ crystals

The growth of FeTe films was conducted in an ultra-high vacuum molecular beam epitaxy (MBE) system with a base pressure about 5×10^{-9} mbar. Sapphire (0001) and STO (100) were used as substrates. Before being transferred to the vacuum system, the sapphire substrate was annealed for one hour at 1223 K in air and the STO (100) substrate was annealed for 2.5 hours in pure oxygen atmosphere after etched in hydrofluoric acid solution to obtain atomically flat and well-defined step-terraces (Figs. S1(a) and S1(d)). Then, FeTe films were prepared by co-depositing high purity Fe (99.98%) and Te (99.9999%) sources from Knudsen cells while the substrate was heated to a suitable temperature. For the films in this study, when using the sapphire (0001) substrate, a Fe:Te flux ratio of approximately 1:12 was used and the growth temperature was set to 623K with a deposition rate of 8 Å/min. When we used the STO (100) substrates, Fe:Te flux ratio was set to 1:4 and the growth temperature was 523K. While in the process of deposition, the growth rate was only determined by the Fe flux.

2. Structural characterization of FeTe films

We have prepared FeTe films on STO (100) and sapphire (0001). The X-ray diffraction (XRD), atomic force microscope (AFM), and transport measurements were used to calibrate the films. Figure S2 shows the XRD peaks in the (00L) direction for FeTe films on different substrates. There were almost no shifts of the 4 peaks' positions of FeTe films compared with bulk. The half-width of the peaks of the films were about 0.26 degree, showing their good crystallization. All of those samples were grown along the FeTe (001) direction regardless of the substrates.

The FeTe films deposited on STO (100) had regular domains, which show symmetric epitaxial growth along the surface step of STO (100) (Figs. S1(b) and S1(c)). Those films show a down-turn in the $R(T)$ curves after oxygen annealing. However, they do not show zero resistance or Meissner effect down to 2 K.

We find that FeTe films grown on sapphire (0001) substrates show different morphologies because of the lattice mismatch (Figs. S1(e) and S1(f)). The domains on sapphire tend to be more disordered regardless of the growth temperature or the flux ratio. After oxygen annealing, only the films with specific interval of growth temperature and flux ratio of Fe:Te show the superconducting behavior we reported.

3. Parameters of the mutual inductance coils

In our experiments, we have used both the coaxially nested mutual inductance coils and split mutual inductance coils with a 30-μm enameled wire. For coaxially nested coils, inner pickup coil with 5000 turns and outer driving coil with 2000 turns were mounted on the same side and coaxially nested. For the split mutual inductance coils, pickup coil with 8000 turns and driving coil with 1500 turns were located on two opposite sides of the FeTe films when performing the measurements. An ac current with frequency between 10 kHz and 20 kHz and amplitude between 1μA and 10 μA was applied to the driving coil and the induced voltage in the pickup coil was measured by a lock-in amplifier.

Appendix B

1. Film thickness and domain size

We prepared FeTe films with different thicknesses on sapphire substrates. As seen from the atomic force microscopy images (Fig. S3), the domain sizes become larger in thicker FeTe films.

2. No magnetic hysteresis is observable in non-superconduting FeTe samples

As a control experiment, we performed mutual inductance measurements on the FeTe films which do not show the zero-resistance superconducting phase down to 2 K (Fig. S4(a)). No Meissner effect is observed from mutual inductance measurement. However, the $R(T)$ curve does still show a sharp down-turn at around 12 K (Fig. S4(a)), suggesting its tendency towards superconductivity. There was no observable magnetic hysteresis from the magnetoresistance (Fig. S4(b)). This could rule out measurement artifacts as a cause of hysteresis in the superconducting samples.

3. The variation of hysteresis with the variation of maximum applied field $H_{\mathbf{max}}$

The magnetic hysteresis data in the main text (Fig. 4(b)) are extracted from the data shown in Figure S5. The linear fitting functions are $y = (-0.01437 \pm 0.00218) + (0.19684 \pm 0.004)x$ and $y = 0.2085 \pm 0.0005$ at small and large H_{max}, respectively. As mentioned in the main text, the crossing point of the two lines determines the penetration field H_{g}. The uncertainties of the fittings are the source of the error bars in Fig. 4(c). When the temperature is at 2 K, the voltage of the out-of-phase component is far larger than that of the in-phase component, and the value of magnetic hysteresis obtained from R_{s} is equal to the minimum value of the out-of-phase component, so $\mu_0 H_{\mathrm{m}}$ could be defined as the minimum point on each line (Fig. S5). The $\mu_0 H_{\mathrm{m}}$ data of the samples with different thicknesses are gathered by the same method.

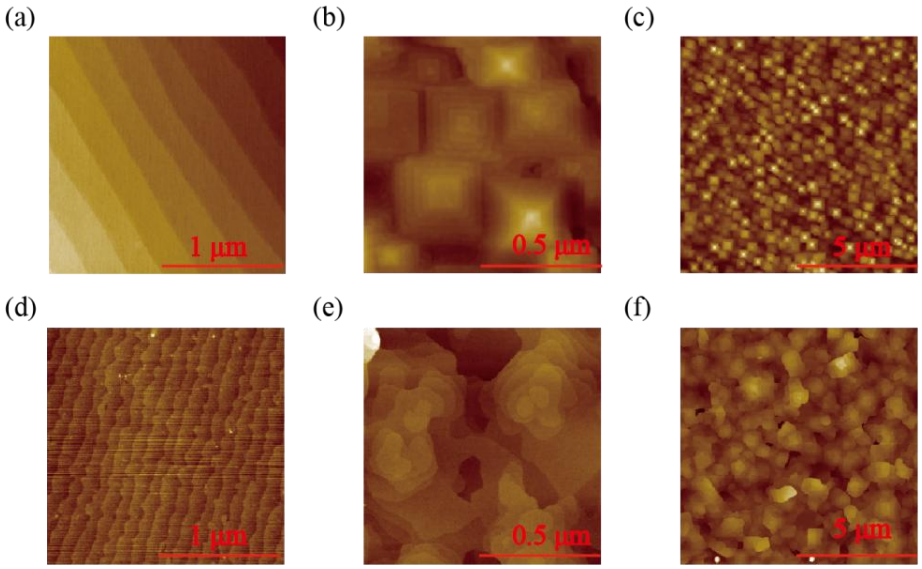

Fig. S1. AFM topographic images of the substrates and FeTe films. (a) and (d) are topographies of $SrTiO_3$ and sapphire substrates, respectively. (b-c) and (e-f) are topographies of FeTe thin films grown on $SrTiO_3$ and sapphire, respectively.

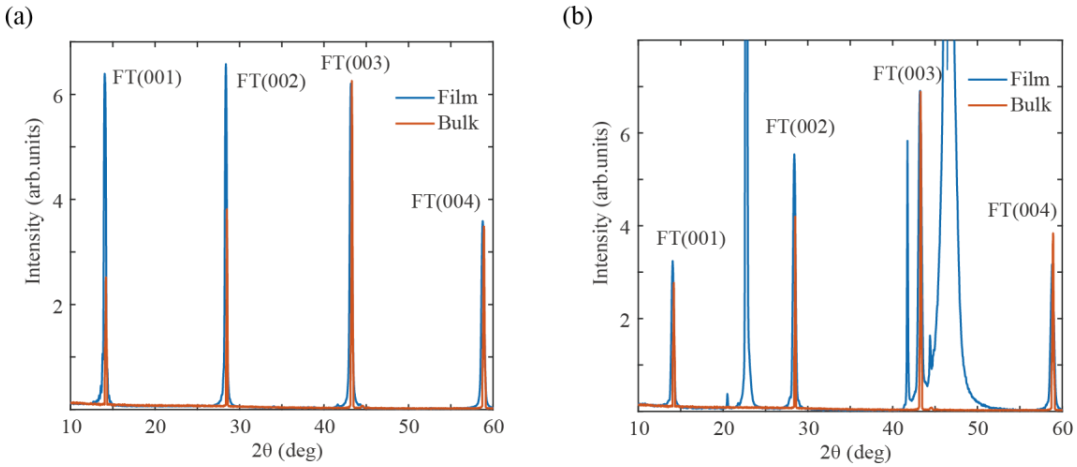

Fig. S2. X-ray diffraction profiles of FeTe bulk and thin films grown on different substrates in comparison with the bulk: (a) on sapphire and (b) on $SrTiO_3$.

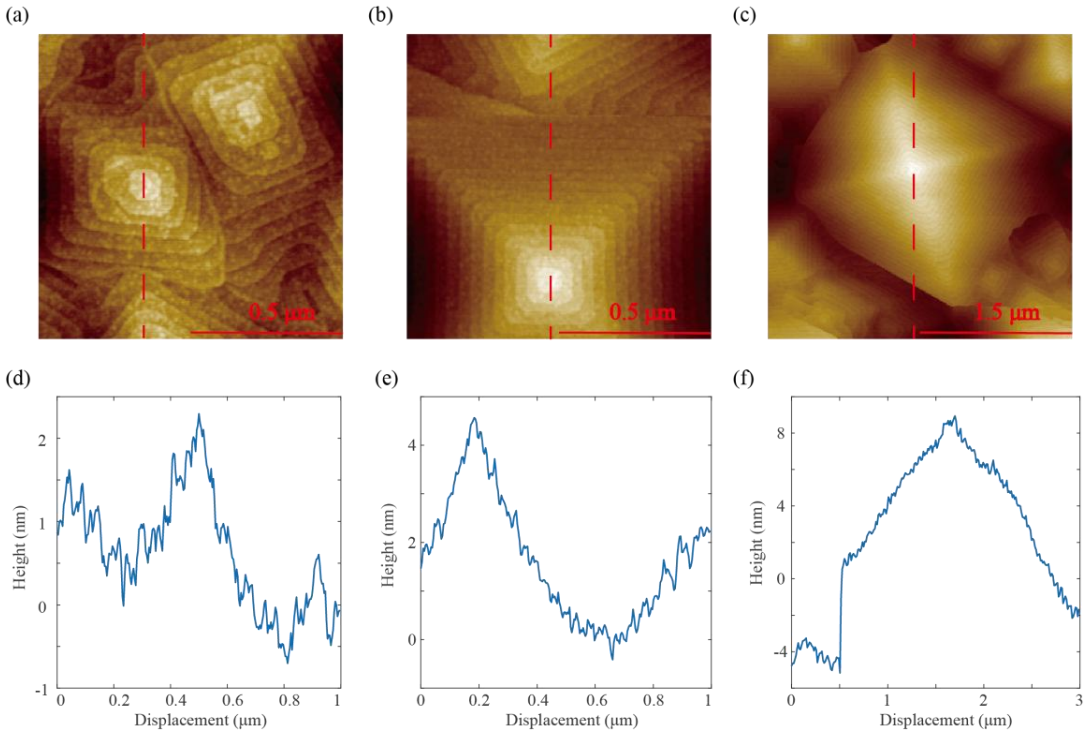

Fig. S3. Atomic force microscope (AFM) images of FeTe films with different thicknesses deposited on the sapphire substrate showing the positive correlation between thickness and roughness. The thicknesses of the films are: 21 nm (a), 53 nm (b) and 88 nm (c). (d-f) The height profiles of the surface topography along the red dashed lines in (a-c), respectively.

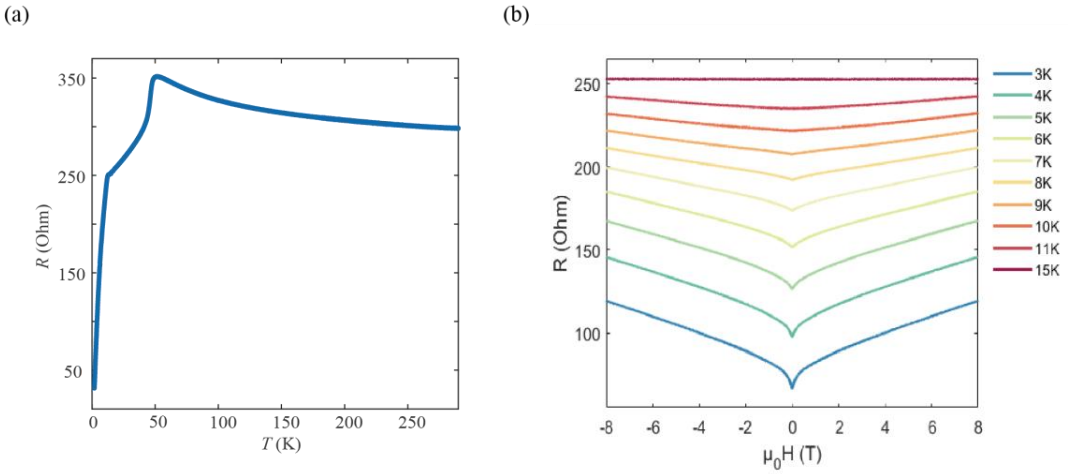

Fig. S4. Non-superconducting FeTe film showing no magnetic hysteresis. (a) Resistance-temperature curve of non-superconducting sample. (b) Field down-sweep and up-sweep of resistance as a function of temperature with $\mu_0 H_{\max}$ = 8 T.

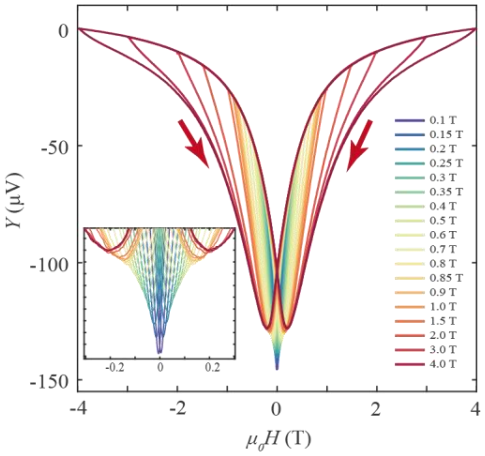

Fig. S5. Out-of-phase component (*Y*) as a function of $\mu_0 H$ measured at 2 K. Inset is a zoom-in of the low field region.